

# MULTIFUNCTIONAL TOPOLOGY DESIGN OF CELLULAR MATERIAL STRUCTURES<sup>1</sup>

**Carolyn Conner Seepersad**  
ccseepersad@mail.utexas.edu  
Mechanical Engineering Department  
The University of Texas at Austin  
Austin, TX 78712

**Janet K. Allen\*, David L. McDowell, and Farrokh Mistree\***  
G. W. Woodruff School of Mechanical Engineering  
Georgia Institute of Technology, Atlanta, GA 30332  
\*and Georgia Tech Savannah, Savannah, GA 31407

## ABSTRACT

Prismatic cellular or honeycomb materials exhibit favorable properties for multifunctional applications such as ultra-light load bearing combined with active cooling. Since these properties are strongly dependent on the underlying cellular structure, design methods are needed for tailoring cellular topologies with customized multifunctional properties. Topology optimization methods are available for synthesizing the form of a cellular structure—including the size, shape, and connectivity of cell walls and openings—rather than specifying these features *a priori*. To date, the application of these methods for cellular materials design has been limited primarily to elastic and thermo-elastic properties, however, and limitations of classic topology optimization methods prevent direct application to many other phenomena such as conjugate heat transfer with internal convection. In this paper, we introduce a practical, two-stage topology design approach for applications that require customized multifunctional properties. In the first stage, robust topology design methods are used to design *flexible* cellular topology with customized structural properties. Dimensional and topological *flexibility* is embodied in the form of robust ranges of cell wall dimensions and robust permutations of a nominal cellular topology. In the second design stage, the flexibility is used to improve the heat transfer characteristics of the design via addition/removal of cell walls and adjustment of cellular dimensions, respectively, without degrading structural performance. We apply the method to design stiff, actively cooled prismatic cellular materials for the combustor liners of next-generation gas turbine engines.

## 1. INTRODUCTION

Materials design involves tailoring the structure and processing path of a material to support its multifunctional role in an engineering application. In this paper, we focus on designing prismatic cellular or honeycomb materials for multifunctional applications that require not only structural performance but also lightweight thermal management capabilities [1,2]. Prismatic cellular materials are particularly well-suited for use as structural heat exchangers because their favorable properties include large surface area density, low pressure drop [3], and in-plane stiffness and strength characteristics that are superior to those of stochastic metal foams [1,4]. The favorable properties of prismatic cellular materials strongly depend on their mesostructural topology, which is characterized by the arrangement, shape, and dimensions of cell openings and

---

<sup>1</sup> This is a revised version of Paper Number DETC2006-99373, published in the *ASME Advances in Design Automation Conference*.



Figure 1. Examples of ordered, prismatic cellular materials.

cell walls.<sup>2</sup> Whereas flexible processing techniques, such as solid freeform fabrication methods [5] or thermo-chemical extrusion processes [6], make it possible to *fabricate* customized cellular mesostructures (as illustrated in Figure 1), methods are needed for *designing* mesostructural topology for multifunctional applications.

Typically, prismatic cellular materials are designed for multifunctional applications by selecting a cellular topology from a small library of standard cellular topologies (e.g., square, triangular, hexagonal, cf. [1]) and modifying cell wall thicknesses to adjust structural and thermal properties [4,7,8]. Alternatively, topology design optimization techniques are used to modify the form of the cellular mesostructure—the size, shape, and connectivity of cell walls and the shape, and arrangement of cell openings—rather than specifying these features *a priori* (cf. [9-11] for recent reviews of topology optimization). To date, topology optimization applications have been limited to customizing the elastic and thermoelastic properties of cellular materials, such as elastic constitutive parameters [12,13], thermal expansion coefficients [14], and effective bulk and shear moduli and conductivity [15].

Multifunctional topology optimization has focused generally on steady state heat conduction [15-17] or to coupled field problems in structural analysis in which the interactions of temperature, electric fields, and/or magnetic fields with deformation are examined for actuators (e.g., [18,19]) or thermoelastic materials (e.g., [14]). These phenomena are governed by mathematical relationships with analogous forms. In contrast, it is unclear how structural topology optimization techniques can be extended for multifunctional applications, such as structural heat exchangers with conjugate heat transfer, that are governed by non-local, scale-dependent phenomena not directly amenable to homogenization or interpolation techniques underlying classic topology optimization methods. To apply topology optimization techniques to structural heat exchangers, for example, the holes or voids that develop in the mesostructure must represent convective channels within the material; however, the properties of each convective channel (e.g., convection coefficients) are highly sensitive to its exact shape, size, depth, and relative position within the mesostructure. These features change as material is redistributed throughout the domain during the topology design process, and they cannot be modeled adequately with local variables (e.g., relative density) and associated effective or homogenized properties in a finely discretized domain. Significant progress has been made, for example, by incorporating topological derivatives [20] within macrostructure topology optimization approaches [9,21-24] to handle Dirichlet and Robin (mixed) boundary conditions on holes. However, important heat transfer characteristics are not considered, including the rate of fluid heating in three dimensional channels and variations in pressure drop, mass flowrate, and convective coefficients with convective channel geometry, with significant inaccuracies for certain applications. More comprehensive multifunctional topology design methods are needed.

In response to these needs, we present a practical, two-stage method for topology design for *multiple* functional domains. The method is outlined for structural heat exchanger design in Figures 2 and 3. In the first stage, robust topology design methods are used to design *flexible*

<sup>2</sup> Length scales are on the order of tens of micrometers to a few millimeters.

topologies with *structural* properties that are robust or relatively insensitive to small changes in the topology or dimensions of the design. In the second stage, this flexibility is leveraged to modify the topology and dimensions of the design and improve its properties in a secondary functional domain (e.g., conjugate heat transfer). The method is intended for rapid exploration of a relatively broad design space with a rich set of multifunctional and robust design objectives. Accordingly, it is paired with approximate, physics-based models for each domain, with more detailed models recommended for further refinement and validation.

A central component in the multifunctional topology design method is the capability for *robust* structural topology design. The robust topology design method itself is a significant extension of both robust design methods and topology design techniques. Robust design methods have been utilized extensively for improving the quality of products and processes by reducing their sensitivity to variation (cf. [25,26]), and in a few cases, for reducing their sensitivity to subsequent changes in the design specifications themselves (e.g., dimensions) [27-30]. However, they have been developed and demonstrated exclusively for applications with *fixed* topology. Previous steps towards robust *topology* design have been limited to

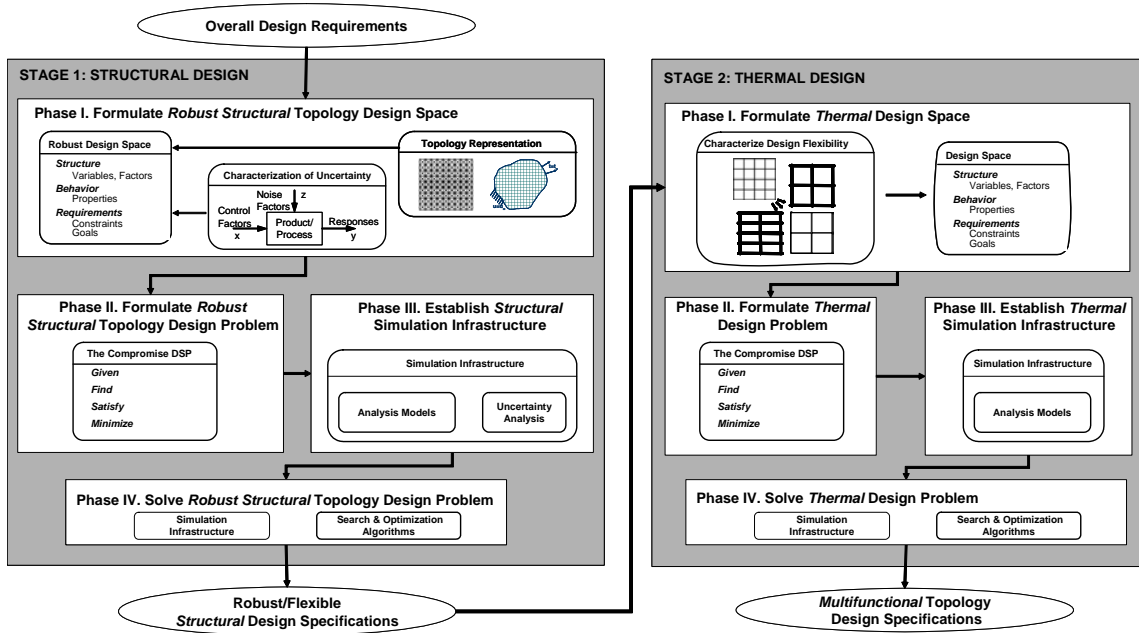


Figure 2. Outline of a two-stage multifunctional topology design method.

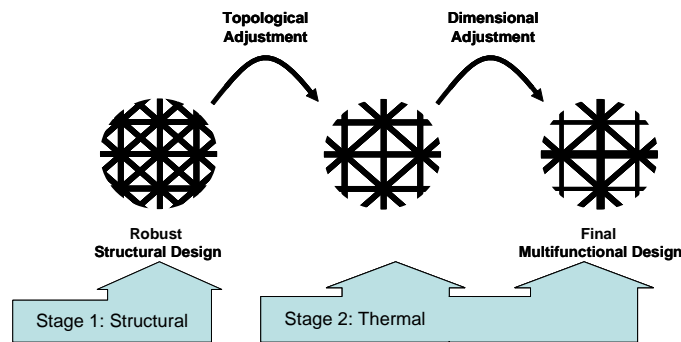


Figure 3. A two-stage multifunctional topology design process.

investigations of the sensitivity of optimal topology to changes in prescribed loads or material properties (e.g., [31-39]). However, these steps are representative of design for mean performance or fail-safe or worst-case design, in which a structure is designed explicitly for worst-case loading, rather than robust design, in which tradeoffs are sought between preferable nominal performance values and minimal sensitivity of performance to uncontrolled variation. Furthermore, partially because topology design was originally focused on full-scale structures rather than materials, variations in the structure itself, such as dimensional or topological imperfections, have not been considered.

In previous work [40,41], we have established a robust topology design method for designing material mesostructures with structural (elastic) properties that are robust to dimensional and topological imperfections—such as dimensional tolerances and missing or cracked cell walls or joints, respectively—that arise in the manufacturing process. In this paper, we show how the robust topology design method can be used to design *multifunctional* topologies, even if non-structural domains cannot be incorporated fully into the structural topology design process. The underlying assumption is that ‘optimal’ *structural* topology design specifications are not necessarily ‘optimal’ or even satisfactory for other functional domains (e.g., conjugate heat transfer) and may benefit from significant modifications to achieve a satisfactory balance among multiple performance measures. Accordingly, we show how the robust topology design method can be used to design structural topologies that are robust to intentional, downstream topological and dimensional adjustments and thereby enable limited topological and parametric design in a subsequent design stage for enhanced performance in an additional functional domain. In the following section, the multifunctional topology design method is described in greater detail along with its application to a motivating example.

## 2. THE MULTIFUNCTIONAL TOPOLOGY DESIGN APPROACH WITH APPLICATION TO A COMBUSTOR LINER EXAMPLE

A motivating example is the design of prismatic cellular materials as combustor liners for next-generation gas turbine engines, as illustrated in Figure 4. In this application, the cellular material acts as a structural heat exchanger—bearing structural loads associated with combustion pressures and thermal expansion and actively cooling itself via forced air convection within the cells. The actively cooled cellular materials are intended to replace standard materials, such as nickel-based superalloys, that require a coating of cool air on combustion-side surfaces to prevent melting, leading to increased emissions and decreased efficiency [42,43]. The design requirements and operating conditions for a ‘mock’ combustor liner example are summarized in Table 1.<sup>3</sup> In summary, the challenge is to design the cellular topology of the combustor liner to achieve a balance of structural properties (compliance and strength at elevated temperatures) and thermal properties (heat transfer rates and cell wall temperatures). In addition, restrictions are placed on wall thickness, volume fraction, and base material to accommodate a thermo-chemical extrusion process for fabricating the prismatic cellular materials [6]. The base material, a Mo-Si-B alloy, is chosen for its high temperature structural properties and amenability for thermo-chemical extrusion [43,44].

---

<sup>3</sup>These requirements are representative of increased temperature in the combustion chamber but do not represent any specific combustor liner application.

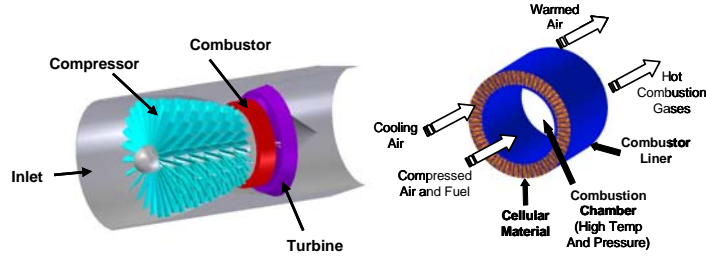


Figure 4. Schematic of a cellular combustor liner.

Table 1. Design requirements and assumptions for the combustor liner application.	
	<p style="text-align: center;"><b>Design Requirements</b></p> <p>Structural</p> <ul style="list-style-type: none"> <li>Minimize compliance function, <math>C</math></li> <li>Stress constraint, <math>S \leq S_y(T)</math></li> </ul> <p>Thermal</p> <ul style="list-style-type: none"> <li>Maximize steady state heat transfer rate, <math>\dot{Q}</math></li> </ul> <p>Fabrication</p> <ul style="list-style-type: none"> <li>Minimum wall thickness, <math>X_i \geq 50 \mu\text{m}</math></li> <li>Maximum volume fraction, <math>v_f \leq 30\%</math></li> </ul>
<p style="text-align: center;"><b>Operating Conditions</b></p> <p> <math>P^*_{\text{gauge}} = P_{\text{interior}} - P_{\text{exterior}} = 100 \text{ MPa}</math>  <math>T_{\text{hot-inner}} = 2000 \text{ K}</math>  <math>T_{\text{max-outer}} \leq 600 \text{ K}</math>  <math>D = 12.7 \text{ cm}</math>  <math>t = 2 \text{ cm}</math>  <math>L = 10 \text{ cm}</math>  <math>T_{\text{in-cooling air}} = 300 \text{ K}</math>  <math>\dot{m}_{\text{in-cooling air}} = 0.64 \text{ kg/s}</math> </p>	<p style="text-align: center;"><b>Base Material</b></p> <p>Mo-Si-B Alloy</p> <p> <math>k = 100 \text{ W/m-K}</math>  <math>\alpha = 6\text{E-}6 \text{ m/m-K}</math>  <math>S_y = 1500 \text{ MPa (@ } 300 \text{ K)}, 400 \text{ MPa (@ } 1650 \text{ K)}</math>  <math>E = 327 \text{ GPa (assumed temperature independent)}</math>  <math>T_{\text{melt-base material}} = 2273 \text{ K}</math> </p>

As illustrated in Figure 2, the multifunctional topology design method is applied to this problem in two distinct stages, corresponding to the governing structural and thermal domains. Each stage is executed in a series of four phases, as described in the rest of this section.

## 2.1 Stage 1: Structural Design

In the structural design stage, the topology of the cellular combustor liner is designed to meet structural performance requirements of minimum compliance and maximum stress levels with flexibility for topological and dimensional adjustment in the subsequent thermal design stage.

### 2.1.1 Phase I: Formulate the Robust Structural Topology Design Space

*Properties of Interest.* As listed in Table 2, the structural properties of interest include the volume fraction,  $v_f$ , of solid cell wall material, the stress in each cell wall,  $S_i$ , and the overall compliance function,  $C$ , of the structure. Since the combustor liner is designed to be robust to potential dimensional and topological changes in the structure, properties include the mean value of the compliance function,  $\mu_C$ , the range of compliance due to dimensional adjustments,  $\Delta_\mu C$ , and the standard deviation of compliance due to specified topological adjustments,  $\sigma_C$ .

Table 2. Summary of design parameters for robust structural topology design of a combustor liner.	
Fixed Factors	<ul style="list-style-type: none"> <li>• Initial ground structure and boundary conditions (Fig. 4)</li> <li>• Material properties (Table 1)</li> </ul>
Sources of Variation	<ul style="list-style-type: none"> <li>• Dimensional adjustments (i.e., changes in in-plane thickness of each cell wall)</li> <li>• Topological adjustments (i.e., removal of cell walls or joints)</li> </ul>
Design Variables	<ul style="list-style-type: none"> <li>• <math>X</math>, Vector of in-plane thicknesses of elements in ground structure</li> </ul>
Properties	<ul style="list-style-type: none"> <li>• <math>v_i</math>, Volume fraction nominal value</li> <li>• <math>S_i</math>, Stress in the <math>i^{\text{th}}</math> element</li> <li>• <math>C</math>, Compliance function for a unit wedge of the combustor liner</li> <li>• <math>\mu_C</math>, Mean value of compliance function</li> <li>• <math>\Delta_{\mu}C</math>, Compliance variation due to dimensional adjustments</li> <li>• <math>\sigma_C</math>, Compliance standard deviation due to topological adjustments</li> </ul>

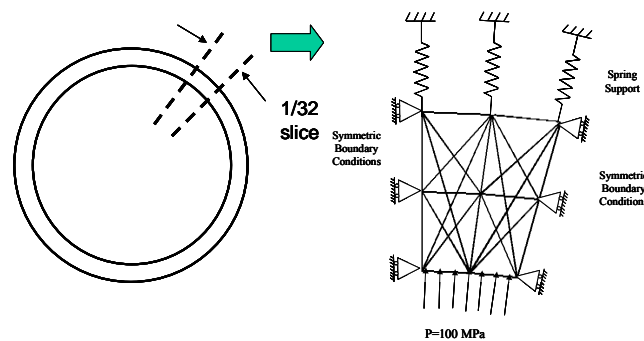


Figure 5. Initial ground structure and boundary conditions for structural topology design.

*Topology Representation and Modification with a Ground Structure.* To establish the topology design domain, the combustor liner is assumed to be axisymmetric and periodic in a basic unit wedge, corresponding to 1/32 of the entire liner, as illustrated in Figure 5. To customize the structural properties of interest, the topology of a unit wedge is represented and modified using a discrete topology design approach based on ground structures (cf. [10,45,46] for reviews, [47] for an introduction, and [12,48,49] for applications). As shown in Figure 5, the ground structure for a single unit wedge is a grid of nodes connected with frame finite elements with six degrees of freedom (cf. [50]).<sup>4</sup> The ground structure is divided into two symmetric halves by a radial plane of symmetry. Within each symmetric half, every pair of nodes is connected with a frame finite element, resulting in a total of 27 elements and 9 nodes. Symmetric boundary conditions are applied to the sides of the unit wedge to simulate the effect of axially symmetric repetition of the unit wedge, and a uniform pressure of 100 MPa is applied to the interior surface. To simulate the elastic constraint of the surrounding engine, the exterior surface is supported by springs with spring constants of approximately 30E8 N/m along the length of the combustor liner. The ground structure density is chosen because it is sufficiently dense to satisfy thermal and structural design requirements; whereas coarser ground structures may restrict the topology design space too much. Results are validated by increasing the number of nodes in the radial and circumferential directions and comparing the results.

<sup>4</sup> Frame finite elements are a superposition of 1D beam and bar finite elements, subject to two displacement and one rotational degree of freedom per node. Frame elements are used to account for transverse loads and bending in cell walls, in addition to axial deformation. Both mechanisms are observed in prismatic cellular materials subject to in-plane loading and elastic deformation.

In the 2D ground structure, a design variable,  $X_i$ , is assigned to the in-plane thickness of each finite element in a symmetric half of the ground structure.<sup>5</sup> The design variables vary between an upper bound,  $X_U$ , on the order of 4000  $\mu\text{m}$  and a lower bound,  $X_L$ , with an extremely small but positive magnitude on the order of 1  $\mu\text{m}$ . After the optimization algorithm converges, elements with in-plane thicknesses near the lower bound are removed to form the final design in a post-processing step in the ground structure method.

*Models of Permissible Dimensional and Topological Adjustments.* Two types of (post-topology optimization) adjustments by a second stage (thermal) designer are considered: (1) dimensional adjustments to the in-plane thickness of each cell wall and (2) topological adjustments in the form of cell wall removal.

*Dimensional adjustment* is defined as a range of potential dimensions,  $\Delta X_i$ , as a function of the nominal in-plane thickness,  $X_i$ , of a cell wall or element as follows:

$$\begin{aligned}\Delta X_i &= X_i - \alpha_1 X_i^{\alpha_2}, \text{ if } X_i \leq 1000 \mu\text{m} \\ \Delta X_i &= 0.1 X_i, \text{ if } X_i > 1000 \mu\text{m}\end{aligned}\tag{1}$$

where  $\alpha_1$  and  $\alpha_2$  are constants with values of 0.502 and 1.085, respectively, and  $X_i$  is measured in  $\mu\text{m}$ . The model in Equation (1) is designed to allow adjustments of approximately +/-30% for a minimum realizable cell wall thickness of 50  $\mu\text{m}$  (in accordance with present thermochemical, extrusion-based processing) and +/-10% for larger dimensions (e.g.,  $\Delta X_i \cong 100 \mu\text{m}$  for  $X_i = 1000 \mu\text{m}$ ). The model in Equation (1) has several desirable properties that aid convergence during the optimization process, including first and second order continuity or smoothness and a guarantee that  $\Delta X_i \leq X_i$  over the entire design space ( $X_L \leq X_i \leq X_U$ ).

*Topological adjustment* is defined as removal of one or more cell walls from the topology in the second design stage. In terms of the ground structure, these adjustments could take the form of removal of individual cell walls (and corresponding elements) or cell joints (and corresponding nodes). Accordingly, we perturb the ground structure in each topology design iteration by sequentially removing each individual node in the ground structure, and the elements attached to it. For computational purposes, we assign a small likelihood that a particular node,  $R_i$ , is removed for thermal design if it is included in the structural topology:

$$\gamma_i = P(R_i \in \mathbf{R}^M \mid R_i \in \mathbf{R}^D)\tag{2}$$

where  $\mathbf{R}^D$  is the set of nodes included in the structural topology (as a subset of the set of nodes in the initial ground structure) and  $\mathbf{R}^M$  is the set of nodes removed for the thermal design.

Several features of these adjustment models are important to note. First, each unit wedge is periodically repeated to create the cellular mesostructure, as illustrated in Figure 5; therefore, we assume that any topological or dimensional adjustments to the unit wedge are repeated periodically throughout the combustor liner.<sup>6</sup> Secondly, these models define the set of *potential* adjustments to be evaluated during the topology design process. The objective of our robust topology design process is to make the final topology robust or insensitive to these adjustments and thereby accommodate a set of potential adjustments that is as broad as possible. At the end of the topology design process, the robust topology is evaluated to determine which specific combinations of elements can be removed from the topology and how much each of the cell wall dimensions can be adjusted, without significantly deteriorating structural properties.

<sup>5</sup> Symmetry implies that changes made in one half are mirrored symmetrically to the other half.

<sup>6</sup> In [40], non-periodic variations in topology are considered.

Accordingly, the outcomes of the robust topology design process include not only a robust topology design but also a detailed list of acceptable adjustments to that particular topology.

### 2.1.2 Phase II: Formulate the Robust Structural Topology Design Problem

In Phase II of the structural design stage, the problem is modeled as a compromise Decision Support Problem—a mathematical model of the multiobjective decision to be solved [51]. The compromise Decision Support Problem (DSP) is a hybrid multiobjective construct that incorporates concepts from both traditional mathematical programming and goal programming [51]. It is used to determine the values of design variables that satisfy a set of constraints and bounds and achieve a set of conflicting, multifunctional goals as closely as possible. The system descriptors, namely, system and deviation variables, system constraints, system goals, bounds and the objective function are described in detail elsewhere [51]. We use the compromise DSP, instead of the deterministic, single-objective, nonlinear programming formulations that are typically used for topology design, because the compromise DSP has several features that facilitate robust topology design. Those features include the capability of accommodating variation in design variables, constraints, and goals and the capability of balancing the multiple objectives associated with meeting targets for multiple material properties and simultaneously minimizing variation in each of those properties.

The compromise DSP is presented in Figure 6, based on the design parameters in Table 2. The design variables are the in-plane thickness,  $X_i$ , of each element in the ground structure. Upper and lower design variable bounds,  $X_U$  and  $X_L$ , are placed on each design variable in Equation (8), and limits,  $v_f\text{-limit}$ , and  $S_y$ , are placed on overall volume fraction,  $v_f$ , and stress in an element, respectively, in Equations (3) and (4). The limits, bounds, and other constants are summarized in Table 3. The goals are formulated in Equations (5) through (7) and include meeting targets for the mean value of a compliance function,  $\mu_C$ , and minimizing the variation in compliance due to dimensional adjustment,  $\Delta_\mu C$ , and topological adjustment,  $\sigma_C$ . Separate goals are included for compliance variation due to dimensional and topological adjustments so that the impact of the two types of adjustments can be assessed and minimized separately. As in goal programming [52], the goals are formulated in terms of achieving target values,  $\mu_{C\text{-target}}$ ,  $\Delta_\mu C_{\text{target}}$ , and  $\sigma_{C\text{-target}}$ , for each goal. Deviation variables,  $d_k^-$  and  $d_k^+$ , measure the extent to which each goal target value is under- or over-achieved, respectively. Each goal formulation is normalized by  $\mu_{C\text{-target}}$  to ensure that the deviation variables range from 0 to 1. Restrictions are included in Equation (9) to limit the deviation variables to positive values and to ensure that only one deviation variable per goal is positively valued at any specific point in the design space [51]. For example, if  $\mu_{C\text{-target}}$  and  $\mu_C$  assume values of 0.5 and 0.25, respectively, in Equation (5), the target value is underachieved rather than overachieved. Accordingly,  $d_i^+$  and  $d_i^-$  are assigned values of 0 and 0.5, respectively, thereby satisfying Equations (5) and (9).

The objective function,  $Z$ , is expressed as a linear, weighted combination of the deviation variables for each goal, as formulated in Equations (10) and (11) for non-robust design and robust design, respectively. Depending on the scenario, one of the objective functions is selected and minimized with the aid of an optimization algorithm. Both weights and goal target values can be adjusted to generate families of solutions that embody a variety of tradeoffs between nominal performance and robustness to dimensional and/or topological adjustments.

---

**Given**

Design space (Sect. 2.1.1); simulation infrastructure (Sect. 2.1.3); targets, bounds, weights (Table 3)

**Find**

$X_i$  In-plane element thickness  $i = 1, \dots, N$  (# elements)

$d_k^-, d_k^+$ , Deviation variables  $k = 1, \dots, 3$

**Satisfy***Constraints*

$$v_f \leq v_{f\text{-limit}} \quad \text{Eq. (3), cf. Eq. (16)}$$

$$S_i \leq S_y \quad \text{Eq. (4), cf. Eq. (15)}$$

*Goals*

$$\frac{\mu_c}{\mu_{c\text{-target}}} + d_1^- - d_1^+ = \frac{\mu_{c\text{-target}}}{\mu_{c\text{-target}}} = 1 \quad \text{Eq. (5), cf. Eq. (22)}$$

$$\frac{\Delta_{\mu} C}{\mu_{c\text{-target}}} + d_2^- - d_2^+ = \frac{\Delta_{\mu} C_{\text{target}}}{\mu_{c\text{-target}}} \quad \text{Eq. (6), cf. Eq. (24)}$$

$$\frac{\sigma_c}{\mu_{c\text{-target}}} + d_3^- - d_3^+ = \frac{\sigma_{c\text{-target}}}{\mu_{c\text{-target}}} \quad \text{Eq. (7), cf. Eq. (23)}$$

*Bounds*

$$X_{i,L} \leq X_i \leq X_{i,U} \quad i = 1, \dots, N \quad \text{Eq. (8)}$$

$$d_k^- \cdot d_k^+ = 0; \quad d_k^-, d_k^+ \geq 0 \quad k = 1, \dots, 3 \quad \text{Eq. (9)}$$

**Minimize**

$$Z = W_1 d_1^+, \quad W_1 = 1 \quad \text{Eq. (10)}$$

$$Z = W_1 d_1^+ + W_2 d_2^+ + W_3 d_3^+, \quad \sum_{k=1}^3 W_k = 1 \quad \text{Eq. (11)}$$

---

**Figure 6. Compromise DSP for robust structural topology design in the combustor liner example.**

<b>Table 3. Design variable bounds, constraint limits, and goal target values for the compromise DSP in Figure 6.</b>	
$v_{f\text{-limit}}$	0.2
$S_y$	600 MPa
$\mu_{c\text{-target}}$	200
$\Delta_{\mu} C_{\text{target}}$	0
$\sigma_{c\text{-target}}$	0
$X_{U}$	4.5 mm
$X_{L}$	0.01 mm
$W_i$ (Eq. 11)	0.33

### 2.1.3 Phase III: Establish Structural Simulation Infrastructure

*Analysis Models.* The analysis model for structural design is based on a finite element model of the structure. Each individual element in the initial ground structure (Figure 5) is modeled as a one-dimensional frame finite element with two nodes and six degrees of freedom—two displacement degrees of freedom per node and one rotational degree of freedom per node. The stiffness matrix for a frame element,  $k_i$ , is obtained from a standard finite element textbook [50,53]. The displacement at each node of the ground structure is obtained by solving the global system of finite element equations for the system [50,53]:

$$[K]\{D\} = \{F\} + \{G\} \quad (12)$$

where  $\{D\}$  is the vector of global displacements,  $\{F\}$  is the vector of applied nodal loads,  $[K]$  is the global stiffness matrix compiled from  $N$  element stiffness matrices,  $k_i$ , and  $\{G\}$  is the vector of loads that account for thermal heating, compiled from  $N$  element matrices,  $g_i$ :

$$\{g_i\} = \alpha_i E_i X_i T_i \{-1 \ 0 \ 0 \ 1 \ 0 \ 0\}^T \quad (13)$$

where  $\alpha_i$ ,  $E_i$ , and  $T_i$  are the coefficient of thermal expansion, modulus of elasticity, and average temperature for element  $i$ . For structural analysis, we assume a uniformly elevated temperature of 950 K and a coefficient of thermal expansion of  $6E-6$ .<sup>7</sup> The rest of the boundary conditions are described in Section 2.1.1.

An overall compliance function for the structure is calculated as follows:

$$C = \sum_{i=1}^N \{d_i\}^T [k_i] \{d_i\} \quad (14)$$

where  $N$  is the total number of elements and  $d_i$  is the vector of displacements associated with element  $i$  due to applied structural and thermal loads. The stress in each element is evaluated as

$$S_i = [E_i] (\{\epsilon_i\} - \{\epsilon_i^o\}) \quad (15)$$

where  $\{\epsilon_i\}$  is the vector of mechanical strains produced by displacements of the nodes and  $\{\epsilon_i^o\}$  is the vector of thermal strains as a function of the coefficient of thermal expansion,  $\alpha$ , for the cell wall material (cf. [53][54]). Finally, the volume fraction of solid material is given by

$$v_f = \frac{1}{A_T} \sum_{i=1}^N X_i L_i \quad (16)$$

where  $A_T$  is the total cross-sectional area of the combustor liner wedge and  $L_i$  is the length of an element. The accuracy of the finite element model is compared with ANSYS models of a representative cellular combustor liner. Stress and displacement values agree within 10-20% for the boundary conditions in Figure 5 and free or fixed displacement on the outer surface (cf. [54]).

*Variability Assessment Models for Evaluating the Impact of Dimensional and Topological Adjustments.* Equation (14) provides nominal properties, but the compromise DSP requires an estimate of the range of the compliance function,  $\Delta C$ , induced by dimensional adjustments and the standard deviation of the compliance function,  $\sigma_c$ , due to topological adjustments. To evaluate the compliance range associated with *dimensional adjustments*, a Taylor series expansion is used:

$$\Delta C = \sum_{i=1}^N \left| \frac{\partial C}{\partial X_i} \Delta X_i \right| \quad (17)$$

To evaluate Equation (17), the partial derivative of the compliance function with respect to the in-plane thickness of an element is calculated as follows, for the specified boundary conditions:

$$\frac{\partial C}{\partial X_i} = -\{d_i\}^T \frac{\partial [k_i]}{\partial X_i} \{d_i\} + 2\{d_i\}^T \frac{G_i}{X_i} \quad (18)$$

In Equation (18), we assume that prescribed loads and displacements are constant and that the second derivative of the compliance function with respect to in-plane thickness of an element is negligible.

---

<sup>7</sup> A constant temperature is assigned during the structural analysis because the actual temperature distribution in the cell walls is unknown prior to thermal analysis.

The impact of *topological adjustments* on the compliance function is evaluated with a series of experiments to simulate the effect of subsequently removing any specific node and its associated elements. If the set of  $D$  nodes in an initial ground structure is expressed as  $\mathbf{R}^D$ , where

$$\mathbf{R}^D = \{R_1, R_2, \dots, R_D\} \quad (19)$$

then a sample space,  $S^j$ , can be defined of possible combinations,  $R^j$ , of  $D$  nodes, selected  $j$  at a time, i.e.,

$$S^j \equiv \{\mathbf{R}^j : \mathbf{R}^j \subseteq \mathbf{R}^D, |\mathbf{R}^j| = j, j \leq D\} \quad (20)$$

For the present case, there are nine nodes (i.e.,  $D = 9$ ) in a single unit wedge of the ground structure in Figure 5. If we assume that any single node may be removed from the structure in the subsequent thermal design stage,  $j$  may be less than  $D$  by a magnitude of one (i.e.,  $j = 8$ ). Therefore, the sample space of nodes,  $S^{j=8}$  includes nine permutations,  $R^{j=8}$ , or possible combinations of the nine nodes, selected eight at a time, namely

$$(R_2, R_3, \dots, R_9), (R_1, R_3, \dots, R_9), \dots, (R_1, R_2, \dots, R_8) \quad (21)$$

where  $R_1$  is the first node,  $R_2$  is the second node, and so on. Therefore, a total of  $V=10$  experiments must be conducted to simulate potential topological adjustments. In the first experiment, the compliance function of the ground structure is evaluated with all of its nodes in place. In the second experiment, the first node is removed from the ground structure, and all of the elements attached to the node are removed from the finite element model. For the third experiment, the first node and its corresponding elements are replaced; the second node and its corresponding elements are removed; and so on until all of the experiments are completed. The compliance function is calculated for each modified ground structure with the finite element model described in this section, modified appropriately for the missing node and elements. For both intact and modified ground structures, symmetric boundary conditions are applied on two sides of the structure, as illustrated in Figure 5. Accordingly, adjustments that appear in a single wedge are assumed to occur periodically in the rest of the combustor liner.

The mean and standard deviation of the compliance function are calculated as

$$\mu_C = \sum_{v=1}^V \gamma_v C(\mathbf{X}_v) \quad (22)$$

$$\sigma_C^2 = \sum_{v=1}^V \gamma_v (C(\mathbf{X}_v) - \mu_C)^2 \quad (23)$$

where  $V$  is the number of experiments in removed nodes,  $X_v$  is the vector of design variables for permutation or Experiment  $v$ , and  $\gamma_v$  is a weight or likelihood assigned to Experiment  $v$  for computational purposes.<sup>8</sup> The value of the weight can be used to adjust the relative contribution of each experiment to the standard deviation metric. In this example, equal weightings are assigned to each node because no *a priori* assumptions are made about which nodes are more likely to be removed. A weight of 0.01 is assigned to the removal of any individual node and a weight of 0.91 to the ground structure with all nodes in place. Since the range of compliance function values associated with dimensional variation is likely to have a different value for each experiment, the mean value for the range of compliance is calculated as follows:

---

<sup>8</sup> The vector of design variables changes for each experiment because a different node is removed in each experiment along with the elements connected to it. Topological robustness,  $\sigma$ , reflects the sensitivity of performance to removal of entire joints (and attached structural elements) as a result of a manufacturing imperfection or intentional removal by a designer for improved performance in a secondary functional domain. In contrast, topological derivatives [20,23,24] measure the sensitivity of performance to insertion of an infinitesimally small hole, and they are more appropriate for continuum topology optimization approaches rather than the discrete approaches adopted in this paper.

$$\Delta_{\mu}C = \sum_{v=1}^V \gamma_v \Delta C(\mathbf{X}_v) \quad (24)$$

Equations (22-24) are used in Equations (5-7) in the compromise DSP of Figure 6. They complete the variability assessment model and simulation infrastructure.

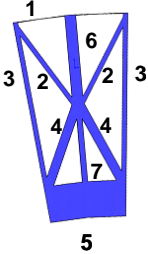
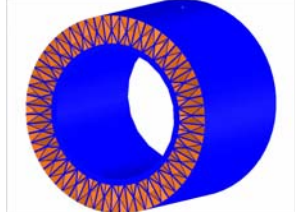
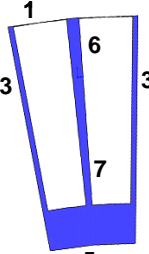
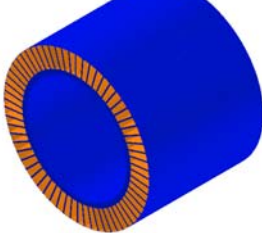
#### 2.1.4 Phase IV: Solve the Robust Structural Topology Design Problem

In the last phase of the structural design stage, the compromise DSP is solved using the simulation infrastructure and the Method of Moving Asymptotes (MMA) algorithm [55]—a gradient-based nonlinear programming algorithm. The resulting unit wedge design is validated and post-processed. In post-processing, elements are removed from the ground structure if their in-plane thicknesses are near the lower bound,  $X_L$ , but no greater than a threshold value of approximately 0.05 mm in this example. The set of elements in the designed structural topology is denoted,  $\phi^S$ , with in-plane thicknesses denoted by  $X^S$ . A space of acceptable topologies,  $\Phi^A$ , is identified to document the set of elements that may be removed from the designed topology,  $\phi^S$ , without significantly impacting structural properties or violating structural constraints. The space,  $\Phi^A$ , can be identified with any of three techniques: (1) Based on the results of experiments in node removal for the final optimization iteration, the designer can identify nodes that can be removed without an unacceptably negative impact on the performance criteria. (2) Based on the final structure, one can use the finite element models to analyze the effect of removing one or more elements from the final robust structure. (3) The robust and non-robust topologies can be compared; often, the non-robust structure is a subset of the robust structure, and redundant elements in the robust structure become candidates for removal. The acceptable range,  $\Delta X^A$ , for the in-plane thickness of each element is also identified based on Equation (1) and documents the freedom for subsequent dimensional adjustment to the structural design.

## 2.2 Structural Results

Robust and non-robust structural designs are reported in the left and right halves of Table 4, respectively. The robust and non-robust structural designs are obtained by solving the compromise DSP in Figure 6 with the objective functions in Equations (11) and (10), respectively. The diagrams depict the designed wedge of cellular mesostructure after post-processing, along with a visualization of the entire combustor liner, created by periodically repeating the wedge in an axisymmetric pattern. Values for all goals are presented in the bottom rows of Table 4 for a single wedge. All of the designs have a 20% volume fraction,  $v_f$ , of solid cell wall material. For the non-robust design,  $\Delta_{\mu}C$  and  $\sigma_c$  are calculated and reported only for comparison purposes because they do not enter the non-robust objective function, Equation (10). The dimensions are reported in terms of nominal values and ranges that correspond to Equation (1). Since each wedge is assumed to be symmetric about a radial axis, dimensions are provided for cell walls in either symmetric half of each wedge.

The robust and non-robust designs have significantly different topologies. The non-robust topology is a reasonable outcome for this problem. Element 5 is needed to support the internal pressure applied by the combustion reaction. Radial elements 3, 6, and 7 are needed to reduce the hoop stresses in the inner cell walls (i.e., Element 5) by transferring some of the load to the outer supports. The robust design includes additional cell walls in Elements 2 and 4. Those cell walls are added as part of the robust topology design process to increase the topological robustness of the structure by providing redundant pathways for transmitting loads from the

Table 4 – Robust and non-robust structural design results.						
ROBUST DESIGN				NON-ROBUST DESIGN		
Cross-Section of a 1/32 Wedge		Complete Combustor Liner		Cross-Section of a 1/32 Wedge		Complete Combustor Liner
						
Element	Nominal Robust Topology, $\phi^s$	Dimension and Range (mm), $X^s \pm \Delta X^s$	Stress (MPa)	Non-Robust Topology	Dimension	Stress (MPa)
1	√	0.1 +/- 0.025	430	√	0.1	430
2	√	0.5 +/- 0.07	360			
3	√	0.5 +/- 0.07	352	√	0.6	536
4	√	1.0 +/- 0.1	379			
5	√	3.7 +/- 0.37	442	√	4.0	430
6	√	1.2 +/- 0.1	525	√	1.3	433
7	√	0.6 +/- 0.08	391	√	1.3	433
Properties of Final Topology		Compliance, C (J)	416	337		
		$\Delta_{\mu}C$	51.0	46.7		
		$\sigma_c$	24.6	37.6		
		Max Stress, S, (MPa)	525	536		

inner surface to the spring-supported outer surface. By comparison with the non-robust structure, the elements are identified as optional and can be removed or added as a topological adjustment in the thermal design stage. The increased topological robustness of the robust design is reflected in the standard deviation of compliance,  $\sigma_c$ , due to topological adjustments, which is substantially lower for the robust design than for the non-robust design. The mean compliance,  $\mu_c$ , of the robust design is slightly higher, a consequence of the tradeoff between minimizing compliance and minimizing sensitivity to topological adjustments. The compliance range due to dimensional adjustments,  $\Delta_{\mu}C$ , is slightly higher for the robust design, reflecting the tolerance stack-up effect of the additional cell walls. Note that the stresses in the cell walls for both designs are relatively low, compared with the yield strength of the material at the reference temperature (cf. Table 1).

For the robust design, the acceptable range of dimensional adjustments for each cell wall is recorded in Table 4, along with the dimensions. The acceptable topological adjustments are represented by the set of acceptable topologies,  $\Phi^A$ , illustrated in Figure 7. All of the derivative topologies exhibit cell wall stresses less than 800 MPa. As shown in the figure, the nominal topology,  $\phi^s$ , may be adjusted topologically by removing Element 2, Element 4, or both. The non-robust topology is also an option; it corresponds to the third acceptable topology in Figure 7. The thermal designer may select any of these options (and adjust their dimensions within the ranges in Table 4) to improve the thermal performance of the design.

The structural results are validated, as reported in [54], by verifying the structural analysis model and the performance of the optimization algorithm. Also, alternative ground structures are investigated by increasing the number of nodes in the radial direction (with no effect) and in the axial direction (with similar results at a smaller scale). For this example, the robust design

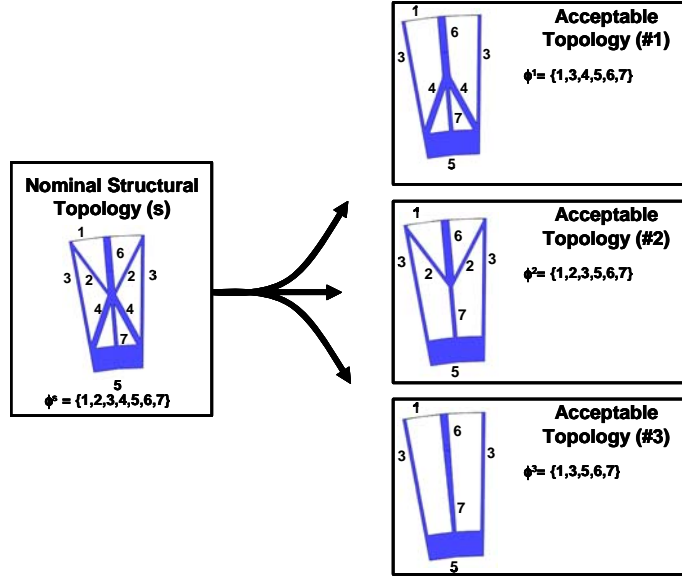


Figure 7. Set of acceptable structural topologies,  $\phi^A$ , derived from the robust structural topology.

algorithm required approximately 50% more computing time than the non-robust algorithm when implemented in Matlab. Although the gap grows linearly with the number of nodes, it is amenable to parallel execution of topological robustness experiments.

## 2.3 Stage 2: Thermal Design

In the thermal design stage, the robust structural design is adjusted to improve its thermal properties. Modifications are limited to the permissible topological and dimensional adjustments identified in the structural design stage.

### 2.3.1 Phase I: Formulate the Thermal Design Space

As documented in Table 5, the thermal properties of interest are the temperature distribution throughout the structure and the total rate of steady state heat transfer from the combustor liner to the cooling air. To adjust these properties, the nominal cellular topology,  $\phi^S$ , and cell wall dimensions,  $X^S$ , from the structural design stage are modified to arrive at a final topology,  $\phi^T$ , and vector of final, in-plane thicknesses of cell walls,  $X^T$ . Dimensions are adjusted within the range of acceptable dimensional adjustments,  $\Delta X^A$ , in Table 4, and cell walls are added/removed within the set of acceptable topologies,  $\phi^A$ , in Figure 7.

Table 5. Summary of design parameters for thermal design of a combustor liner.	
Fixed Factors	<ul style="list-style-type: none"> <li>Boundary conditions</li> <li>Material properties</li> <li>Nominal topology, <math>\phi^S</math>, and dimensions, <math>X^S</math>, Table 4</li> </ul>
Bounds on Permissible Adjustments	<ul style="list-style-type: none"> <li><math>\Delta X^A</math>, Dimensional adjustments (i.e., changes in in-plane thickness of each cell wall)</li> <li><math>\phi^A</math>, Topological adjustments (i.e., removal of cell walls or joints), Figure 7, Table 4</li> </ul>
Design Variables	<ul style="list-style-type: none"> <li><math>X^T</math>, Vector of final in-plane thicknesses of elements (cell walls)</li> <li><math>\phi^T</math>, Final topology</li> </ul>
Properties	<ul style="list-style-type: none"> <li><math>T_i</math>, Average temperature in the element <math>i</math></li> <li><math>\dot{Q}</math>, total rate of steady state heat transfer</li> </ul>

---

**Given**

Thermal design space (Sect. 2.3.1)  
Simulation infrastructure (Sect. 2.3.3)  
Targets, bounds, weights (Table 6)

**Find**

$X_i^T$  In-plane element thickness  $i = 1, \dots, N$   $N = \# \text{ elements in final topology, } \mathcal{X}^T$   
 $\phi^T$  Set of elements in final topology  
 $d_k^-, d_k^+$  Deviation variables  $k = 1, \dots, 3$

**Satisfy***Constraints*

$v_f \leq v_{f\text{-limit}}$  Eq. (3), cf. Eq. (16)  
 $\phi^T \in \Phi^A$  Eq. (25), cf. Figure 7

*Goals*

$\frac{\dot{Q}}{\dot{Q}_{\text{target}}} + d_1^- - d_1^+ = \frac{\dot{Q}_{\text{target}}}{\dot{Q}_{\text{target}}} = 1$  Eq. (26), cf. Eq. (36)

*Bounds*

$X_{i,L} \leq X_i \leq X_{i,U}$   $i = 1, \dots, N$  Eq. (27), cf. Tables 4, 6, Eq. (1)

$d_k^- \cdot d_k^+ = 0$ ;  $d_k^-, d_k^+ \geq 0$   $k = 1, \dots, 3$ ; Eq. (9)

**Minimize**

$Z = W_1 d_1^-, W_1 = 1$  Eq. (28)

---

**Figure 8. Compromise DSP for robust structural topology design in the combustor liner example.**

<b>Table 6. Design variable bounds, constraint limits, and goal target values for the compromise DSP in Figure 9.</b>	
$v_{f\text{-limit}}$	$\cong 0.25$
$\dot{Q}_{\text{target}}$	10 kW
$X_U$	$X_{i,U} = X_i^s + \Delta X_i$ , cf. Table (4) and Eq. (1)
$X_L$	$X_{i,L} = X_i^s - \Delta X_i$ , cf. Table (4) and Eq. (1)
$W_i$ (Eq. 28)	1.0

### 2.3.2 Phase II: Formulate the Thermal Design Problem

The compromise DSP for thermal design is documented in Figure 8. Corresponding constraint limits, goal target values, and weights are listed in Table 6.

### 2.3.3 Phase III: Establish the Thermal Simulation Infrastructure

Heat transfer analysis is performed using a hybrid finite element/finite difference approach for approximating the temperature distribution in the cellular mesostructure and the total rate of steady state heat transfer from the cellular heat sink to the fluid flowing through its passageways. Although detailed FLUENT models can provide the same information, the approximate finite element/finite difference models are faster, more easily reconfigurable, and share a common representation with the structural finite element models. These features facilitate rapid exploration of a broad design space and direct importation of structural designs. Once those

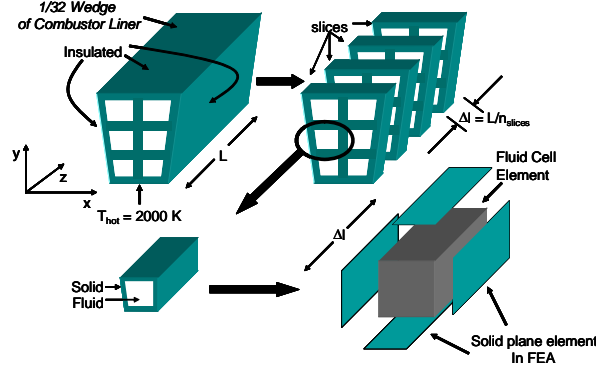


**Figure 9. Finite element analysis of a thermal ground structure.**

regions are identified, more accurate, computationally expensive simulations (e.g., FLUENT) can be used for subsequent detailed design and confirmation of properties.

As shown in Figure 9, a single wedge of the prismatic cellular material in the combustor liner is analyzed. The thermal boundary conditions for the wedge include a heated inner (bottom) surface with fixed temperature,  $T_{hot-inner} = 2000$  K, which we assume is reduced to 1700 K by a thin ceramic coating on the inner, combustion-side surface of the combustor liner. The left, right and outer (top) surfaces are insulated, and the entry and exit surfaces are exposed to convective flow at an inlet air temperature,  $T_{in-cooling\ air}$ , of 300 K and mass flowrate,  $\dot{m}_{in-cooling\ air}$ , of 0.64 kg/s or 0.02 kg/s per unit wedge. The wedge is divided into slices at regular intervals,  $\Delta l$ , in the  $z$ -direction in Figure 9, with the interval determined by a grid convergence study. Within each slice, each solid cell wall is modeled as a 2D, linear, planar finite element, and each fluid passageway is modeled as a fluid cell, as illustrated in Figure 9. The topological arrangement of the solid elements in each slice corresponds precisely to the arrangement of elements in the structural design,  $\phi^S$ , that forms the starting point for the thermal design process.

By modeling the cell walls with 2D planar elements, we assume that the cell walls are thin and that temperature gradients across the transverse thickness of a cell wall are negligible; in return, we achieve considerable computational savings relative to fully three-dimensional finite element or CFD analysis. Heat conduction in the direction of fluid flow is assumed to be negligible—an assumption that permits division of the finite element model into slices along its length in the  $z$  direction in Figure 9.

The finite element model for the solid walls of the heat sink is derived from the governing equation for steady state heat transfer in a two-dimensional plane system and Newton's Law of Cooling for the balance of energy transfer across element boundaries due to conduction and convection [50,56]. The cell wall material is assumed to be isotropic. The thermal conductivity of solid cell wall material is assigned a constant value and normalized to account for the transverse thickness,  $X_i$ , of each cell wall. Each finite element has in-plane length,  $a$ , and in-plane depth,  $b$ , equivalent to the length of a slice,  $\Delta l$ . We assume that each lateral surface has a uniform surface temperature,  $T_{wall}^i$ , calculated as the average of nodal temperatures for the element, and a uniform heat transfer coefficient,  $\beta_1$  or  $\beta_2$ . Based on these assumptions, the finite element equations in matrix form reduce to the following :

$$\left[ \left[ K_{th}^i \right] + \left[ H_{th}^i \right] \right] \{ T^i \} = \left[ F_{th}^i \right] + \left[ P_{th}^i \right] \quad (29)$$

where  $[K_{th}^i]$ ,  $[H_{th}^i]$ ,  $[F_{th}^i]$ , and  $[P_{th}^i]$  are the conductivity matrix, boundary convection matrix, heat flux vector, and boundary convection vector. Details of the model are available in [54], as derived from [50]. At least two adjoining elements of depth,  $\Delta l$ , are used to model each cell wall in each slice (with a cell wall spanning two neighboring joints). Additional elements are used to account for conduction through the inner ring surface of the combustor liner, as described in [54]. By applying appropriate boundary conditions and assembling the element equations (Equation (29)), a finite element model of the heat sink walls is formulated.

For evaluating convective boundary conditions and the total rate of steady state heat transfer, fluid cell elements are used to model the behavior of convective fluid in each cell passageway, as illustrated in Figure 9. The dimensions of each fluid cell are determined by the arrangement and thicknesses of neighboring solid cell wall elements and by the length,  $\Delta l$ , of each slice. Fully developed turbulent flow is assumed in each fluid cell. The temperature in each incremental fluid cell is assumed to be constant, and the fluid temperature difference in a fluid cell from inlet to exit is assumed to be very small. Fluid properties for each incremental fluid cell are evaluated at the inlet temperature based on curve fits to tabulated data available in handbooks or textbooks (e.g.,[56]). The inlet fluid temperature,  $T_{in-cooling\ air}$ , is assumed constant over the entire cross-section of the structure. The mass flowrate of air in each fluid cell is determined with a momentum balance calculation [57] in which the pressure head is equalized for each cell. The pressure drop,  $\Delta P$ , across the heat sink is calculated with the Darcy-Weisbach formula, which is equivalent to the pressure head multiplied by the fluid density [56]:

$$\Delta P_i = f_i \frac{\rho_{inlet} L}{D_{H_i}} \left( \frac{V_i^2}{2} \right) \quad (30)$$

where  $f_i$ ,  $\rho_{inlet}$ ,  $L$ ,  $D_{H_i}$ , and  $V_i$  are the Darcy friction factor, mean fluid density at the heat sink inlet, combustor liner length, hydraulic diameter, and mean fluid velocity, respectively, for the  $i^{\text{th}}$  fluid cell. For turbulent flow, the Darcy friction factor,  $f$ , and the Nusselt number,  $Nu$ , are functions of the Reynolds number,  $Re$ , and Prandtl number,  $Pr$  [56]:

$$f_i = (0.790 \ln(Re_{D_i}) - 1.64)^{-2} \quad (31)$$

$$Nu_{D_i} = \frac{(f_i/8)(Re_{D_i} - 1000)Pr_i}{1 + 12.7(f_i/8)^{1/2}(Pr_i^{2/3} - 1)} \quad (32)$$

The Nusselt number is used to calculate the convective coefficient,  $\beta_i$ , for the fluid cell as follows [56]:

$$Nu_{D_i} = \frac{\beta_i D_{H_i}}{k_i} \quad (33)$$

where  $k_i$  is the conductivity of the fluid medium. The hydraulic diameter,  $D_H$ , is updated to reflect iterative changes in the thicknesses of surrounding walls. The convective coefficient for the  $i^{\text{th}}$  incremental fluid cell can be used to calculate the change in mean fluid temperature between the entrance ( $T_{in_i}$ ) and the outlet ( $T_{exit_i}$ ) of the incremental fluid cell as a function of the surface area of the incremental fluid cell,  $A_{s_i}$ , mean wall temperature of the solid material enclosing the fluid cell,  $T_{wall_i}$ , mass flowrate of fluid in the incremental fluid cell,  $\dot{m}_i$ , and the specific heat of the fluid,  $c_{p_i}$ , evaluated at  $T_{in_i}$ :

$$T_{out_i} = T_{wall_i} - (T_{wall_i} - T_{in_i}) \exp\left(\frac{-\beta_i A_{s_i}}{\dot{m}_i c_{p_i}}\right) \quad (34)$$

The mean wall temperature is obtained by solving an assembly of element equations (Eq. (29)) for the nodal temperatures in the heat sink and averaging the nodal temperatures for each solid cell wall element. We assume that the outlet temperature of an incremental fluid cell becomes the inlet temperature of the corresponding fluid cell in the next slice. The rate of steady state heat transfer,  $\dot{Q}_i$ , from heat sink walls to a fluid cell is calculated as follows:

$$\dot{Q}_i = \dot{m}_i c_{p_i} (T_{in_i} - T_{out_i}) \quad (35)$$

The *total* rate of steady state heat transfer,  $\dot{Q}$ , is obtained by summing the contributions from each cell,  $i$ , for each incremental slice,  $j$ , of the structure:

$$\dot{Q} = \sum_{j=1}^{\# \text{ slices}} \sum_{i=1}^{\# \text{ cells}} \dot{Q}_i^j \quad (36)$$

The total rate of steady state heat transfer is maximized to lower the temperature within the cell walls. Lowering the temperature within the cell walls is important because the yield strength is a function of the temperature of the base material, as noted in Table 1.

The thermal analysis model is validated by comparison with FLUENT simulations for a test case that is representative of the geometries and boundary conditions reflected in the final design. Results indicate that the temperatures and total rates of steady state heat transfer are accurate within 25% and that the approximate model is approximately two orders of magnitude faster than the FLUENT analysis [54].

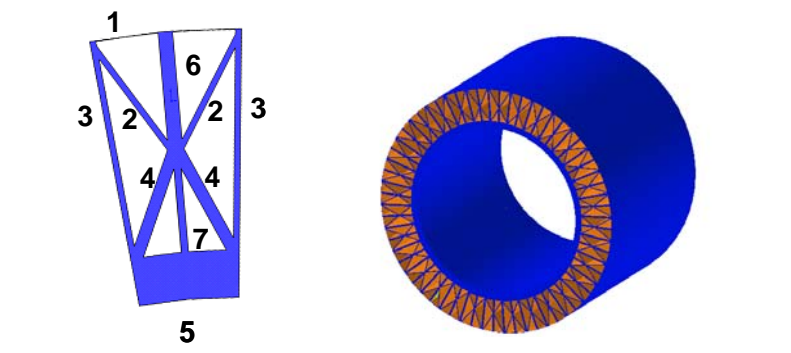
#### 2.3.4 Phase IV: Solve the Thermal Design Problem

Like the structural problem, the thermal design problem is solved with an MMA algorithm. For efficiency and effectiveness of the gradient-based algorithm, approximations of the analytical gradients of the total rate of steady state heat transfer are calculated [54].

## 2.4 Thermal Design Results

The thermal design process begins with the results of the robust *structural* design stage. First, the thermal properties of each of the acceptable topologies,  $\Phi^A$ , are evaluated, and the topology that exhibits the highest rate of steady state heat transfer and lowest cell wall temperatures is identified. The topology and corresponding properties are recorded in the left half of Table 7. Then, the dimensions of the selected topology are modified within the range of acceptable dimensional adjustments,  $\Delta X^A$ , to improve the total rate of steady state heat transfer, and the improved properties are recorded in the right half of Table 7. The properties of the non-robust structural design are evaluated and recorded in Table 8. The non-robust design serves as a benchmark because it is indicative of the thermal properties obtainable *without* opportunities for dimensional or topological adjustment. Both robust and non-robust designs are feasible because maximum cell wall temperatures (limited to 1700 K by a ceramic lining) and average temperatures at the outlet are sufficiently low to withstand estimated cell wall stresses and prevent melting, according to the material properties in Table 1.

**Table 7. Thermal design results for robust design from Table 4. Thermal design modifications are limited to acceptable topological and dimensional adjustments.**

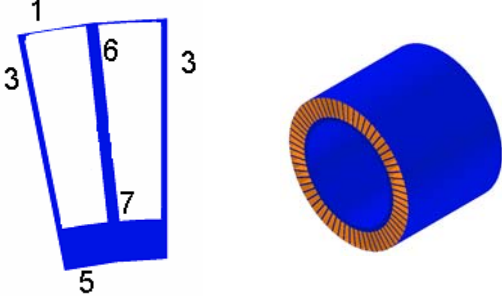


Nominal Design				Design Modified within Ranges			
Element	Dim. and Range (mm), $X^e \pm \Delta X^A$	Avg. Temp. Outlet (K), $T$	Stress (MPa), $S$	Element	Final Dim. (mm), $X$	Avg. Temp. Outlet (K), $T$	Stress (MPa), $S$
1	0.1 +/- 0.025	634	427	1	0.09	656	411
2	0.5 +/- 0.07	724	356	2	0.57	750	316
3	0.5 +/- 0.07	949	355	3	0.57	962	314
4	1.0 +/- 0.1	1173	385	4	1.1	1183	356
5	3.7 +/- 0.37	1541	433	5	4.0	1527	427
6	1.2 +/- 0.1	769	543	6	1.3	795	502
7	0.6 +/- 0.08	1207	401	7	0.68	1220	362
$\dot{Q}$ , Total Rate of Steady State Heat Transfer (W)			4027	$\dot{Q}$ , Total Rate of Steady State Heat Transfer (W)			4095
$C$ , Compliance			418	$C$ , Compliance			469

From a thermal perspective, the differences between the non-robust and robust topologies are noteworthy. First, the additional cell walls in the robust design have a significant impact on its thermal properties, increasing the total rate of steady state heat transfer by nearly 50% and lowering the temperature (hence, raising the yield strength) in each of the cell walls relative to the non-robust design. On the other hand, the structural properties are not degraded significantly, relative to the non-robust benchmark design, with stress levels remaining relatively consistent, on average, and compliance increasing by approximately 20%. The thermal properties of the robust design are improved further by modifying its dimensions, as recorded in the right half of Table 7. Because the dimensions are increased or decreased to the allowable bounds, it is likely that further increases in heat transfer rate would be obtainable with broader bounds, but the tradeoffs are likely to include slightly higher average wall temperatures, as observed in the data in Table 7. While the effects of dimensional adjustments are noticeable, with a nearly 2% increase in heat transfer rate, the magnitude is much lower than the effects of the topological adjustments, suggesting that flexibility for topological adjustments is a key ingredient in a successful multifunctional topology design method.

The improved performance of the robust design is not coincidental. Although the non-robust topology satisfies structural performance goals most closely, redundant cell walls are included purposefully in the robust design to expand options for topological adjustment in the thermal design stage. With the robust structural topology design process, thermal design options include not only the non-robust topology, but also at least three alternative topologies, as illustrated in Figure 7, and a range of cell wall dimensions for each one.

**Table 8. Thermal properties of the non-robust, benchmark design from Table 4.**



Non-Robust Design			
Element	Dimension, X	Avg. Temp. @ Outlet(K), T	Stress (MPa), S
1	0.1	781	430
3	0.6	1080	536
5	4.0	1642	430
6&7	1.3	1103	433
$\dot{Q}$ , Total Rate of Steady State Heat Transfer (W)			2499
C, Compliance			342

The thermostructural design results are validated with a two-dimensional, thermostructural ANSYS analysis of a single wedge of the final design in Table 7. Boundary conditions include an internal pressure of 100 MPa, an external pressure of 68.5 MPa (to simulate the impact of surrounding support structure), symmetric boundary conditions on the sides of the wedge, and uniform temperatures applied to each cell wall, according to the temperatures documented in Table 7. Four-node, linear, quadrilateral elements (PLANE42) are applied, with at least 3 elements through the in-plane thickness of each cell wall and material properties according to Table 1. Results indicate average stress levels of 100-200 MPa in the inner ring and less than 600 MPa in the rest of the mesostructure. Since the yield strength of Mo-Si-B alloys is reported to range from 400 MPa at an elevated temperature of 1650K to 1500 MPa at 350K, the proposed cellular material design should meet the design requirements. The results indicate that actively-cooled cellular combustor liners are promising candidates for withstanding the temperatures and pressures of a next-generation combustion chamber.

**3. CLOSURE**

A two-stage method is presented for multifunctional topology design applications that demand not only targeted structural performance but also satisfactory performance in a distinct secondary functional domain. Intended secondary domains, such as conjugate heat transfer, are governed by non-local, scale-dependent phenomena that are not directly amenable to standard homogenization or interpolation techniques underlying discrete or continuum topology optimization techniques. For this class of applications, conventional approaches involve either selecting a standard topology or identifying a final topology via conventional *structural* topology optimization and thereby fixing its topology for subsequent *multifunctional* customization. Instead, we advocate a two-stage approach for multifunctional topology design in which both topology and dimensions are adjusted for multifunctional performance requirements. For the first stage, we devise a robust structural topology design process for designing a preliminary topology with structural performance that meets targets as closely as possible while remaining relatively insensitive to bounded adjustments in the topology itself and its dimensions. In the

second stage, the topology is modified, within the acceptable bounds, to improve its multifunctional performance in a secondary domain. The method incorporates approximate physics-based models that facilitate rapid exploration of a broad design space and identification of promising multifunctional solutions that are verified subsequently with more detailed models.

The two-stage method is applied to design the cellular mesostructure of prismatic cellular (honeycomb) materials for an actively cooled combustor liner in a next-generation gas turbine engine. The example requires *both structural and thermal performance* in terms of stiffness and strength to support combustion pressures and total rates of steady state heat transfer and associated cell wall temperatures to increase the temperature-dependent strength of the cell wall material. In this example, we use the two-stage multifunctional topology design method to generate a *flexible* structural topology that may be adjusted topologically and parametrically via adding/removing specific cell walls and increasing/decreasing the dimensions of each cell wall, respectively. Then, we leverage the acceptable adjustments to meet thermal performance objectives as closely as possible. As a result of the robust structural topology design process, we find that the flexible structural design is more complex than a benchmark, non-robust design and incorporates several redundant or optional cell walls and potential ranges of cell wall dimensions. This topological and parametric flexibility leads to improved thermal performance. Currently, the approach is based on a discrete, ground structure-based topology design method. It would be interesting to consider the use of robustness for multifunctional topology design with other topology design techniques such as the bubble method or level set method with topological gradients. Also, it would be interesting to simultaneously consider additional sources of variability (such as material properties or loading) and its impact on sensitivity to failure due to yielding, buckling, and other mechanisms.

The method and the example have important *materials design implications*. The method should be broadly applicable for multifunctional topology design that involves structural performance goals combined with additional multifunctional phenomena—such as conjugate heat transfer, catalysis, or transport—that are not amenable to standard structural topology optimization techniques. In addition, the robust design methods should be effective for managing dependencies between distributed materials design activities that are partitioned between disciplines, stages, or expert designers. Using robust design methods, designers can preserve topological and dimensional freedom for subsequent adjustment of intermediate designs. Consequently, in many cases it is possible to identify satisfactory multifunctional solutions without prolonged, sequential iteration between stages, disciplines, or designers and without computationally intractable centralized design for multiple functional domains. Furthermore, the method and its accompanying example provide strong evidence for the utility and effectiveness of systematic and strategic materials design methods. In this case, the preliminary conclusion is that prismatic cellular materials with a base material of Mo-Si-B intermetallic can be designed to withstand the temperatures and pressures of a high performance combustion chamber *without* combustion-side air cooling (as required by metal alloys and superalloys), thereby reducing emissions and increasing engine efficiency. The results make us optimistic that systematic approaches for concurrent design of products and materials are effective for devising solutions to advanced, materials-limited applications that have challenged materials scientists for decades. In this paper, we have targeted mesostructural length scales in the design of multifunctional structures using pre-selected base materials; we envision tremendous potential for extending these design methods for smaller length scales, as well.

## ACKNOWLEDGMENTS

Financial support from NSF DMI-0632766 and DMI-0600474 at the University of Texas at Austin and AFOSR MURI (1606U81), NSF DMI-0085136, and DMI-0407627 at Georgia Tech is gratefully acknowledged. During her graduate study at Georgia Tech, Carolyn Conner Seepersad was sponsored by a National Science Foundation Graduate Fellowship and a Hertz Foundation Fellowship. Krister Svanburg of the Royal Institute of Technology in Stockholm, Sweden, kindly supplied a MATLAB version of his MMA algorithm.

## REFERENCES

1. Hayes, A. M., A. Wang, B. M. Dempsey and D. L. McDowell, 2004, "Mechanics of Linear Cellular Alloys," *Mechanics of Materials*, Vol. 36, No. 8, pp. 691-713.
2. Evans, A. G., J. W. Hutchinson and M. F. Ashby, 1999, "Multifunctionality of Cellular Metal Systems," *Progress in Materials Science*, Vol. 43, No. 3, pp. 171-221.
3. Lu, T. J., 1999, "Heat Transfer Efficiency of Metal Honeycombs," *International Journal of Heat and Mass Transfer*, Vol. 42, No. 11, pp. 2031-2040.
4. Evans, A. G., J. W. Hutchinson, N. A. Fleck, M. F. Ashby and H. N. G. Wadley, 2001, "The Topological Design of Multifunctional Cellular Materials," *Progress in Materials Science*, Vol. 46, No. 3-4, pp. 309-327.
5. Beaman, J. J., J. W. Barlow, D. L. Bourell, R. H. Crawford, H. L. Marcus and K. P. McAlea, 1997, *Solid Freeform Fabrication: A New Direction in Manufacturing*, Kluwer Academic Publishers, Boston.
6. Cochran, J. K., K. J. Lee, D. L. McDowell and T. H. Sanders, 2000, "Low Density Monolithic Honeycombs by Thermal Chemical Processing," *Proceedings of the 4th Conference on Aerospace Materials, Processes, and Environmental Technology*, Huntsville, AL.
7. Seepersad, C. C., B. M. Dempsey, J. K. Allen, F. Mistree and D. L. McDowell, 2004, "Design of Multifunctional Honeycomb Materials," *AIAA Journal*, Vol. 42, No. 5, pp. 1025-1033.
8. Seepersad, C. C., R. S. Kumar, J. K. Allen, F. Mistree and D. L. McDowell, 2005, "Multifunctional Design of Prismatic Cellular Materials," *Journal of Computer-Aided Materials Design*, Vol. 11, No. 2-3, pp. 163-181.
9. Eschenauer, H. A. and N. Olhoff, 2001, "Topology Optimization of Continuum Structures: A Review," *Applied Mechanics Reviews*, Vol. 54, No. 4, pp. 331-389.
10. Ohsaki, M. and C. C. Swan, 2002, "Topology and Geometry Optimization of Trusses and Frames," *Recent Advances in Optimal Structural Design* (S. A. Burns, Ed.), American Society of Civil Engineers, Reston, VA.
11. Soto, C., 2001, "Structural Topology Optimization: From Minimizing Compliance to Maximizing Energy Absorption," *International Journal of Vehicle Design*, Vol. 25, No. 1/2, pp. 142-160.
12. Sigmund, O., 1994, "Materials with Prescribed Constitutive Parameters: An Inverse Homogenization Problem," *International Journal of Solids and Structures*, Vol. 31, No. 17, pp. 2313-2329.
13. Sigmund, O., 1995, "Tailoring Materials with Prescribed Elastic Properties," *Mechanics of Materials*, Vol. 20, No. 4, pp. 351-368.

14. Sigmund, O. and S. Torquato, 1997, "Design of Materials with Extreme Thermal Expansion Using a Three-Phase Topology Optimization Method," *Journal of the Mechanics and Physics of Solids*, Vol. 45, No. 6, pp. 1037-1067.
15. Hyun, S. and S. Torquato, 2002, "Optimal and Manufacturable Two-Dimensional, Kagome-Like Cellular Solids," *Journal of Materials Research*, Vol. 17, No. 1, pp. 137-144.
16. Li, Q., G. P. Steven, Y. M. Xie and O. M. Querin, 2004, "Evolutionary Topology Optimization for Temperature Reduction of Heat Conducting Fields," *International Journal of Heat and Mass Transfer*, Vol. 47, No. 23, pp. 5071-5083.
17. Li, Q., G. P. Steven and O. M. Querin, 2000, "Structural Topology Design with Multiple Thermal Criteria," *Engineering Computations*, Vol. 17, No. 6, pp. 715-734.
18. Sigmund, O., 2001, "Design of Multiphysics Actuators Using Topology Optimization -- Part I: One-Material Structures," *Computer Methods in Applied Mechanics and Engineering*, Vol. 190, No. 49-50, pp. 6577-6604.
19. Sigmund, O., S. Torquato and I. A. Aksay, 1998, "On the Design of 1-3 Piezocomposites Using Topology Optimization," *Journal of Materials Research*, Vol. 13, No. 4, pp. 1038-1048.
20. Sokolowski, J. and A. Zochowski, 1999, "On the Topological Derivative in Shape Optimization," *SIAM Journal of Control Optimization*, Vol. 37, pp. 1251-1272.
21. Eschenauer, H. A., V. V. Kobelev and A. Schumacher, 1994, "Bubble Method for Topology and Shape Optimization of Structures," *Structural and Multidisciplinary Optimization*, Vol. 8, No. 42-51.
22. Burger, M., B. Hackl and W. Ring, 2004, "Incorporating Topological Derivatives into Level Set Methods," *Journal of Computational Physics*, Vol. 194, pp. 344-362.
23. Novotny, A. A., R. A. Feijoo, E. Taroco and C. Padra, 2003, "Topological Sensitivity Analysis," *Computer Methods in Applied Mechanics and Engineering*, Vol. 192, pp. 803-829.
24. Cea, J., S. Garreau, P. Guillaume and M. Masmoudi, 2000, "The Shape and Topological Optimization Connection," *Computer Methods in Applied Mechanics and Engineering*, Vol. 188, No. 4, pp. 713-726.
25. Taguchi, G., 1986, *Introduction to Quality Engineering*, Asian Productivity Organization, UNIPUB, White Plains, NY.
26. Phadke, M. S., 1989, *Quality Engineering Using Robust Design*, Prentice Hall, Englewood Cliffs, NJ.
27. Chang, T. S. and A. C. Ward, 1995, "Conceptual Robustness in Simultaneous Engineering: A Formulation in Continuous Spaces," *Research in Engineering Design*, Vol. 7, No. 2, pp. 67-85.
28. Chang, T. S., A. C. Ward, J. Lee and E. H. Jacox, 1994, "Conceptual Robustness in Simultaneous Engineering: An Extension of Taguchi's Parameter Design," *Research in Engineering Design*, Vol. 6, pp. 211-222.
29. Chen, W. and K. Lewis, 1999, "A Robust Design Approach for Achieving Flexibility in Multidisciplinary Design," *AIAA Journal*, Vol. 37, No. 8, pp. 982-989.
30. Kalsi, M., K. Hacker and K. Lewis, 2001, "A Comprehensive Robust Design Approach for Decision Trade-Offs in Complex Systems Design," *ASME Journal of Mechanical Design*, Vol. 123, No. 1, pp. 1-10.
31. Diaz, A. and M. P. Bendsoe, 1992, "Shape Optimization of Structures for Multiple Loading Situations Using a Homogenization Method," *Structural Optimization*, Vol. 4, No. 1, pp. 17-22.

32. Diaz, A., R. Lipton and C. A. Soto, 1995, "A New Formulation of the Problem of Optimum Reinforcement of Reissner-Mindlin Plates," *Computer Methods in Applied Mechanics and Engineering*, Vol. 123, No. 1-4, pp. 121-139.
33. Maute, K. and D. M. Frangopol, 2003, "Reliability-Based Design of MEMS Mechanisms by Topology Optimization," *Computers and Structures*, Vol. 81, No. 8-11, pp. 813-824.
34. Thampan, C. K. P. V. and C. S. Krishnamoorthy, 2001, "System Reliability-Based Configuration Optimization of Trusses," *Journal of Structural Engineering*, Vol. 127, No. 8, pp. 947-956.
35. Bae, K.-R., S. Wang and K. K. Choi, 2002, "Reliability-Based Topology Optimization," *9th AIAA/ISSMO Symposium on Multidisciplinary Analysis and Optimization*, Atlanta, GA. Paper No: AIAA-2002-5542.
36. Ben-Tal, A. and A. Nemirovski, 1997, "Robust Truss Topology Design via Semidefinite Programming," *SIAM Journal of Optimization*, Vol. 7, No. 4, pp. 991-1016.
37. Cherkhaev, A. and E. Cherkhaeva, 1999, "Optimal Design for Uncertain Loading Conditions," *Homogenization* (V. Berdichevsky, V. Jikov and G. Papanicolaou, Eds.), World Scientific, pp. 193-213.
38. Kocvara, M., J. Zowe and A. Nemirovski, 2000, "Cascading--An Approach to Robust Material Optimization," *Computers and Structures*, Vol. 76, No. 1-3, pp. 431-442.
39. Sandgren, E. and T. M. Cameron, 2002, "Robust Design Optimization of Structures through Consideration of Variation," *Computers and Structures*, Vol. 80, No. 20-21, pp. 1605-1613.
40. Seepersad, C. C., J. K. Allen, D. L. McDowell and F. Mistree, 2006, "Robust Design of Cellular Materials with Topological and Dimensional Imperfections," *ASME Journal of Mechanical Design*, *In Press*.
41. Seepersad, C. C., J. K. Allen, D. L. McDowell and F. Mistree, 2003, "Robust Topological Design of Cellular Materials," *ASME Advances in Design Automation*, Chicago, IL. Paper No. DETC2003/DAC-48772.
42. Bailey, J. C., J. Intile, T. F. Fric, A. K. Tolpadi, N. V. Nirmalan and R. S. Bunker, 2002, "Experimental and Numerical Study of Heat Transfer in a Gas Turbine Combustor Liner," *International Gas Turbine Conference and Exposition*, Amsterdam, Netherlands. ASME. Paper Number: GT-2002-30183.
43. Dimiduk, D. M. and J. H. Perepezko, 2003, "Mo-Si-B Alloys: Developing a Revolutionary Turbine-Engine Material," *MRS Bulletin*, Vol. September, pp. 639-645.
44. Schneibel, J. H., M. J. Kramer, O. Unal and R. N. Wright, 2001, "Processing and Mechanical Properties of a Molybdenum Silicide with the Composition Mo-12Si-8.5B (at. %)," *Intermetallics*, Vol. 9, No. 1, pp. 25-31.
45. Kirsch, U., 1989, "Optimal Topologies of Structures," *Applied Mechanics Reviews*, Vol. 42, No. 8, pp. 223-239.
46. Topping, B. H. V., 1984, "Shape Optimization of Skeletal Structures: A Review," *Journal of Structural Engineering*, Vol. 109, No. 8, pp. 1933-1951.
47. Dorn, W. S., R. E. Gomory and H. J. Greenberg, 1964, "Automatic Design of Optimal Structures," *Journal de Mecanique*, Vol. 3, pp. 25-52.
48. Frecker, M. I., G. K. Ananthasuresh, S. Nishiwaki, N. Kikuchi and S. Kota, 1997, "Topological Synthesis of Compliant Mechanisms Using Multi-Criteria Optimization," *ASME Journal of Mechanical Design*, Vol. 119, No. 2, pp. 238-245.

49. Pedersen, C. B. W., 2003, "Topology Optimization Design of Crushed 2D-Frames for Desired Energy Absorption History," *Structural and Multidisciplinary Optimization*, Vol. 25, No. 5-6, pp. 368-382.
50. Reddy, J. N., 1993, *An Introduction to the Finite Element Method*, 2nd Ed., McGraw-Hill, Boston.
51. Mistree, F., O. F. Hughes and B. A. Bras, 1993, "The Compromise Decision Support Problem and the Adaptive Linear Programming Algorithm," *Structural Optimization: Status and Promise* (M. P. Kamat, Ed.), AIAA, Washington, D.C., pp. 247-286.
52. Charnes, A. and W. W. Cooper, 1961, *Management Models and Industrial Applications of Linear Programming*, John Wiley & Sons, New York, NY.
53. Cook, R. D., D. S. Malkus and M. E. Plesha, 1989, *Concepts and Applications of Finite Element Analysis*, 3rd Ed., John Wiley and Sons, New York.
54. Seepersad, C. C., 2004, "A Robust Topological Preliminary Design Exploration Method with Materials Design Applications," *PhD Dissertation*, G.W. Woodruff School of Mechanical Engineering, Georgia Institute of Technology, Atlanta, GA.
55. Svanberg, K., 1987, "The Method of Moving Asymptotes--A New Method for Structural Optimization," *International Journal for Numerical Methods in Engineering*, Vol. 24, No. 2, pp. 359-373.
56. Incropera, F. P. and D. P. DeWitt, 1996, *Fundamentals of Heat and Mass Transfer*, 3rd Edition Ed., John Wiley & Sons, New York.
57. Hodge, B. K., 1999, *Analysis and Design of Energy Systems*, Simon & Schuster, Upper Saddle River, NJ.